Spring 5-2016

Synthesis of Acceptors for Use in Donor-Acceptor Copolymers and Characterization of these Polymers

William D. Walker
University of Southern Mississippi

The University of Southern Mississippi

Synthesis of Acceptors for Use in Donor-Acceptor Copolymers and Characterization of these Polymers

by

William Walker

A Thesis
Submitted to the Honors College of
The University of Southern Mississippi
in Partial Fulfillment
of the Requirements for the Degree of
Bachelor of Science
in the School of Polymers and High Performance Materials

May 2016

Approved by

Jason D. Azoulay, Ph.D., Thesis Adviser
Assistant Professor of Polymer Science and Engineering

Sarah Morgan, Ph.D., Director
School of Polymers and High Performance Materials

Ellen Weinauer, Ph.D., Dean
Honors College

Abstract

In this thesis, a selenium-derivatized acceptor was synthesized to examine the heavy atom effects of selenium on the position of the frontier molecular orbitals (HOMO/LUMO band gap) as opposed to sulfur in a donor-acceptor copolymer for use in light harvesting and detection applications. Over the course of this research, standard operating protocols for ultraviolet-visible (UV-Vis-NIR) and Fourier transform infrared (FT-IR) spectroscopies, as well as cyclic voltammetry (CV) characterization techniques were established. Once synthesized, the polymers were characterized through use of the established characterization protocols. The selenium-derivatized polymer exhibited a bathochromic shift compared to the sulfur analogue, with a solid-state absorption cutoff of 1140 nm compared to 1050 nm for the sulfur analogue and an optical band gap of ~1.1 eV.

Key Words: polymer, infrared light harvesting, donor-acceptor copolymer, selenium, band gap

Acknowledgements

I would sincerely like to thank Dr. Jason Azoulay, my research advisor, for his mentoring and guidance over the last two years. I was given the unique opportunity to work directly with him, rather than with a graduate student, throughout my time in the lab. Through this experience, I have gained a plethora of skills that most undergraduate researchers would not have had the opportunity to acquire. Dr. Azoulay has been extremely generous with his knowledge in the field of donor-acceptor copolymers and organic photovoltaics. I wish to extend a special thank you to Alex London for his assistance and advice on my various endeavors in the lab. I also wish to Dr. James Rawlins for the time spent in his research group and the skills that I acquired there.

I am extremely grateful for the constant support in academics and all areas of life from my parents, John and Melinda Walker, and my sister, Ashlynn Walker. I would also like to thank my uncle, Michael Blanton, for first sparking my interest in polymers and science in general.

I wish to acknowledge the University of Southern Mississippi Center for Undergraduate Research for support and funding of this project.

Table of Contents

List of Tables

List of Equations, Figures and Schemes

EQUATIONS

FIGURES

SCHEMES

List of Abbreviations

BHJ	Bulk Heterojunction
DA	Donor-Acceptor
OPV	Organic Photovoltaic
IR	Infrared
UV-Vis	Ultraviolet-Visible Spectrophotometry
FT-IR	Fourier Transform Infrared Spectrophotometry
CV	Cyclic Voltammetry
NMR	Nuclear Magnetic Resonance Spectroscopy

Chapter I: Introduction

Sensing light from the ultraviolet (UV)–visible throughout the infrared (IR) portions of the electromagnetic spectrum forms the foundation for a wide variety of scientific and technological applications. Conjugated polymers that effectively produce and harvest visible light find use in a variety of commercially relevant optoelectronic technologies offering new manufacturing paradigms.[1-13] There is currently considerable interest in expanding the scope of these materials to afford functionality in the IR spectral regions to make new devices and applications possible.[14-21] The development of these materials has thus far been limited by a lack of direct ways to tailor structural, electronic, and optical properties with an appropriate degree of synthetic precision, prohibiting further study and generation of new materials. Donor-acceptor (DA) conjugated copolymers made from alternating electron-rich (donor) and poor (acceptor) moieties have emerged as the dominant class of high performance light harvesting materials and offer properties not attainable in conjugated homopolymers, such as the well-known poly(3-hexylthiophene) (P3HT).[23] These materials exhibit improved charge separation and charge transport efficiencies, high chemical stability, strong absorption profiles that can be adjusted across a wide wavelength (λ) range, and properties that can be readily tuned through chemical modification.[24-31] Whereas many strategies exist to modify the properties of conjugated materials, molecular species with absorption profiles above 1 μm (comparable to the absorption cut off of silicon) are relatively rare, difficult to access, and generally exhibit low optical sensitivity. The requisite to form a type-II (staggered) heterojunction with appropriately positioned energy levels and maintain a suitable energetic offset between materials sets further complicates identifying combinations to harness longer λ light.

Recent efforts in the Azoulay group have involved identifying structural and electronic properties for obtaining modular narrow band gap DA copolymers with properties suitable for harvesting longer λ light (Figure 1). The following research uses these modular synthetic approaches to produce materials with variable band gaps and molecular configurations in order to study applications for photodetection/sensing in the near-IR (0.9–1.4 μm), short-wavelength IR (1.4–3 μm), and mid-wavelength IR (3–8 μm) spectral regions. This research also focuses on the development of characterization protocols to determine the viability of these materials in their intended applications. Protocols for UV-Vis and FT-IR spectroscopy techniques were developed to analyze the absorption profiles for these materials and cyclic voltammetry (CV) protocol was developed to assess the position of the frontier orbital energies.

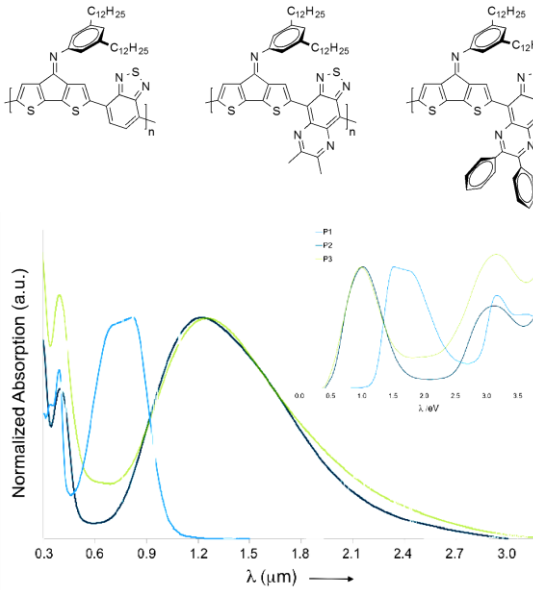

Figure 1. (Top) Molecular structures of polymers **P1**–**P3** with progressively narrow band gaps. (Bottom) UV-Vis-NIR absorption spectra of **P1**–**P3** as a thin-film and AM1.5G solar photon flux highlighting atmospheric transmittance windows. Figure adopted from reference [22]

Chapter II. Literature Review

2.1 Basis for Synthetic Procedures

In response to the world's rapidly increasing need for renewable energy, significant research attention has been placed on harvesting energy directly from the sun by using photovoltaic devices. One low cost option for producing clean, renewable energy is polymer solar cells (PSCs). These devices are desirable for many applications, as they have the potential to be fabricated onto large lightweight, flexible substrates via solution processing.[32, 33]

Initial research into the field of organic photovoltaic (OPV) cells consisting of an active layer between two electrodes resulted in materials with very inefficient power conversion due to a lack of charge carrier generation.[35] In order to improve conversion and transport properties for use in photovoltaic applications, Tang developed what is known as bilayer heterojunction approach by using what is known as a p-type layer for hole transport combined with an n-type layer for electron transport.[36] As shown in Figure 2, the general working principle in such solar cells first involves the photoexcitation of the donor material by the absorption of light to generate excitons. The general principle by which these solar cells operate involves an excitation in the donor material from photon absorption to generate excitons (bound states of electrons and electron holes bound by Coulombic attraction). This exciton then diffuses to the donor-acceptor (D-A) interface, at which point the exciton dissociates via an electron-transfer process. Once fully separated, the free charge carriers are transported to the respective electrodes in the opposite direction with the aid of an internal electric field. This process in turn generates the photocurrent and photovoltage. Excitons can only diffuse short distances between 5 and 14 nm due to

their short lifetimes, therefore any excitons created at a distance from the heterojunction interface decay back to the ground state before reaching the acceptor.[37-41] This leads to a loss of absorbed photons and low quantum efficiency. As such, devices based on bilayer heterojunctions have limited efficiencies due to the small charge-generating interfacial area between the donor and acceptor components.

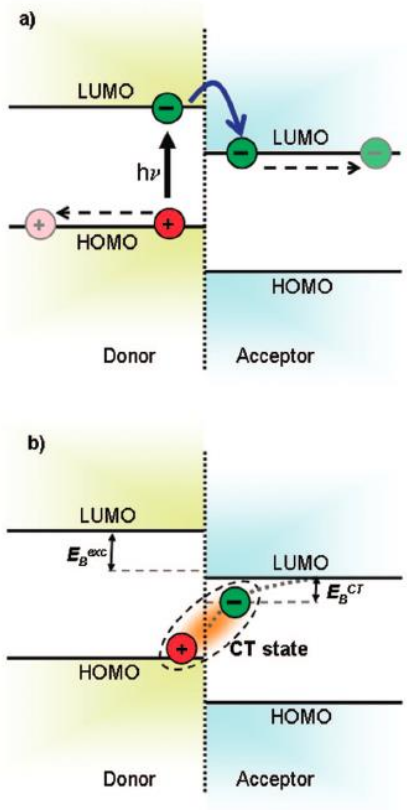

Figure 2: A) Simplified illustration of photoexcitiation of electron from donor HOMO into donor LUMO and subsequent transfer into acceptor LUMO at D-A interface. B) Illustration of electron-hole pair (exciton) formed on the D-A interface. Figure adopted from reference [34].

Blending donor and acceptor materials together creates an interpenetrating D-A network with a large interfacial area known as a bulk heterojuction (BHJ). This blending can be achieved through controlling the phase separation between the donor and acceptor components in bulk, producing materials in which there is always a donor-acceptor interface within a few nanometers of any photoabsorbing site in the composite. This composition leads to enhanced efficiencies of charge separation. This research led to the formation of bicontinuous networks, creating two channels to transport holes in the donor domain and two channels to transport electrons in the acceptor domain, resulting in efficient charge collection.

Due to the BHJ D-A configuration consisting of only single active layer to create an internal D-A heterojunction, device fabrication can be greatly simplified through solution processing techniques. These fabrication techniques eliminate the problems with

interfacial erosion encountered when making bilayer configuration devices. The typical architecture of a BHJ solar cell is shown in Figure 3, where the active layer is sandwiched between two electrodes.

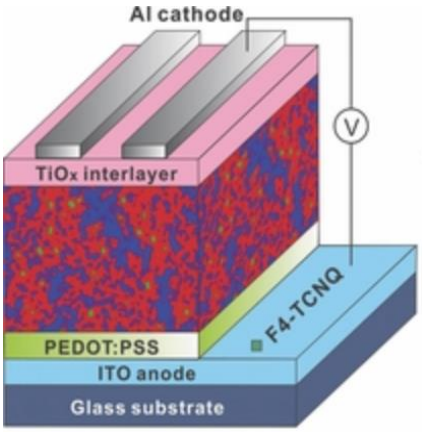

Figure 3. A generalized example of a bulk heterojunction in a solar cell. Adopted from reference [42].

Bulk heterojunction solar cell research underwent rapid developments after a major breakthrough, in which Sariciftci and coworkers discovered efficient photo-induced electron transfer in conjugated polymer-fullerene composites.[43] Buckminsterfullerene (C60) proves to be an ideal n-type material for several reasons. First, Buckminsterfullerene's lowest unoccupied molecular orbital (LUMO) is relatively low-lying, and thus energetically favorable in terms of accepting electrons from an excited p-type material.[44] Second, the C60 LUMO is triply degenerate, enabling it to be reduced by up to six electrons, uniquely stabilizing negative charges. Third, electron transfer from a conjugated polymer to C60 occurs on a very rapid (femtosecond) timescale. This transfer is faster than the radiative decay of photoexcitation back or back electron transfer by several orders of magnitude. Due to the increasingly short electron transfer times of conjugated polymers, the quantum efficiency of charge separation approaches unity.[45] An ultrafast electron transfer such as this immediately quenches the highly reactive excited state of p-type materials, allowing any possible photo-oxidation associated with oxygen to be reduced. This characteristic greatly improves the photostability of the conjugated polymers.[46, 47] Finally, C60 derivatives also exhibit very high electron mobilities.[48] However, C60 derivatives tend to crystallize

and are not very soluble in organic solvents, hindering direct applications in inexpensive solution-based processing techniques. The only way around this is to functionalize C60 with solubilizing moieties.[49-53] [6,6]-phenyl-C61-butyric acid methyl ester (PCBM), first synthesized by researchers Wudl and Hummelen in 1995, is the most universally used acceptor for modern BHJ solar cell studies .[53] The structural symmetry of PCBM, however, inhibits low-energy transitions, therefore limiting its absorption in the visible light region. Bulk heterojunction devices can be made more efficient by replacing C60 PCBM acceptors with the higher fullerene analogue C70 PCBM (PC71BM),[54, 55] which has lower symmetry and absorbs more visible light.[56] The enhancement provided by C70 can be mainly attributed to its stronger light absorption in the visible region than C60.

Current cutting-edge polymer photodetectors exhibit a broad spectral response of 300–1,450 nm and high detectivities (10^{12}–10^{13} cm $Hz^{0.5}$ W^{-1}), which work to afford performance characteristics better than their inorganic-based counterparts when operating at room temperature. The optical sensitivity in the NIR is due to a long absorption tail emanating from vibronic features within the molecular species and as such limits the achievable performance. These problems in developing materials with desired performance has motivated the development of inorganic-organic hybrid devices using polymeric and small-molecule materials in conjunction with II–VI quantum dots (EQE < 1% at $\lambda > 1$ μm) or single-walled carbon nanotubes (EQE ≈ 2% at $\lambda = 1.15$ and 1.3 μm). Fused porphyrins can be modified to exhibit a longer λ response by spatially extending the conjugation of the π-electron system, but suffer from low efficiencies of charge separation, difficulties associated with synthesis, limited utility, and therefore only result in low EQEs (6.5 % at $\lambda = 1.35$ μm). As a result of these inefficiencies, photodetection in the information-rich

0.9–2.6 μm spectral region can only be done via solid-state inorganic-based devices. These inorganic systems are limited in terms of modularity, are fragile by nature, require cooling below room temperature to perform reasonably, and are largely incompatible with traditional silicon CMOS (complementary metal–oxide–semiconductor) processes. Solution-processable photodetectors that operate at room temperature would be a completely innovative and important technology. The development of this technology will rely on revolutionary breakthroughs primarily in the availability of new materials and careful control over the physical properties.

In order to develop materials with the optical and electronic properties of traditional inorganic semiconductors, but with added processing advantages, there is much research attention on the development of conjugated polymers. In addition to being used in a wide variety of applications such as in organic conductors, field-effect transistors and electroluminescent diodes, conjugated polymers continue to serve as the most promising p-type materials for producing organic solar cells with low weight, intrinsic flexibility, and low cost. Over the past decade, a sizeable research effort has been focused on creating numerous novel conjugated polymers. As a result of this research effort, device performance in BHJ solar cells has continuously increased. Materials with PCEs of 8-10 % are commonplace among newly developed low band gap conjugated polymers, a result encouraging to the field. The structural evolution of such materials is shown in Figure 4.

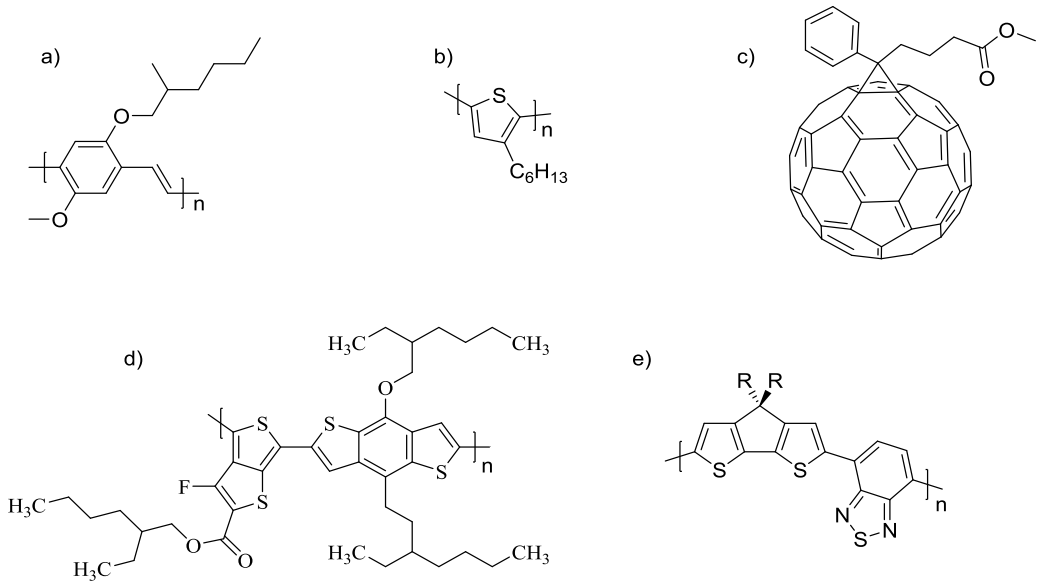

Figure 4. Development of materials used in OPVs: a) MEH-PPV, b) P3HT donor used in conjunction with c) PCBM acceptor. High-performance D-A copolymers: d) PTB7 e) PCPDTBT

A promising class of DA copolymers combines 4*H*-cyclopenta[2,1-*b*:3,4-*b'*]dithiophene (CPDT) and 2,1,3-benzothiadiazole (BT) (Figure 4, structure e).[57] This polymer exhibits ideal properties for warranting further studies, such as intermediate EQEs with photoresponsivity extending into the NIR, high detectivities (>10^{13} cm $Hz^{0.5}W^{-1}$) in solution-processed photodetectors,[58] well-established photophysical properties, and a comprehensive picture of the interfacial energy landscape in combination with [60]PCBM,[59] however, a systematic investigation of some of the most relevant properties is not possible.

The proposed research seeks to combine CPDT donors with 2,1,3-benzoselenadiazole (BSe) in order to assess the effects of the heavier chalcogen atom on the band gap. Recent studies have shown the merit in using selenophene or other selenium derivatized donor-acceptor systems as opposed to strictly thiophene-based systems. These selenium-derivatized systems exhibited higher stability in the oxidized state, red-shifted

absorption profiles, and a lower optical band gap when compared to the thiophene analogues.[60-62] Though sulfur and selenium (and heavier chalcogens such as tellurium) possess similar chemical properties, such as electronegativity, the heavier chalcogens have a larger atomic radius and are, therefore, more polarizable. Likewise, the selenium analogues of corresponding sulfur compounds are more polarizable and have larger dipole moments due to the larger selenium atom.[63,64] Further studies have shown that substitution of selenium analogues in D-A systems can be used to tune the band gap and optical properties.[65-68] The proposed research seeks to copolymerize a BSe acceptor with a proprietary donor moiety based on CPDT.

2.2 Mechanisms of Characterization

In order to assess the viability of these materials for use in light harvesting and energy generation applications, their absorption and electrical properties must be characterized. Organic photovoltaic conversion requires that the optical excitation energy be equal to the incident photon energy, i.e. the optical band gap of the material must match the energy of the wavelength of incident light. Rather than generating a free electron and an electron hole, organic photovoltaics generate a tightly bound exciton (electron/hole pair). Since the traditional electronic band gap refers to energy gap between free holes at the valence band and free electrons in the conduction band of inorganic semiconductors, the optical band gap is often more appropriate for organic materials.[69] The optical band gap can be related to the electronic band gap with the exciton binding energy through the expression in Equation 1, where E_{gap} is the electronic band gap (measured through cyclic voltammetry), E_{opt} is the optical band gap (measured through spectrophotometry), and E_B

is the exciton binding energy, or the energy required to separate the electron and hole in an exciton into a radical ion pair.[70]

$$E_{gap} = E_{opt} + E_B$$

Equation 1. Relation of electronic band gap to optical band gap.[70]

2.2.1 Spectrophotometry

Though most organic functional groups are transparent in the UV-vis region of the electromagnetic spectrum, absorption spectroscopy in this region can be very useful for assessing the optical properties of materials used for light harvesting applications. UV-vis absorption spectroscopy measures how much light is absorbed by a transparent sample at a given wavelength and quantifies these absorptions relative to a certain wavelength established as zero absorption. When energy is absorbed by the sample, molecules transition from a low energy ground state to a a higher energy excited state. The difference between these two states is equal to the energy of the radiation absorbed to cause the transition. The most probable transition observed in UV-Vis-NIR spectroscopy is the promotion of an electron from the HOMO to the LUMO. The onset of this transition indicates the optical band gap of the analyte.

Occupied molecular orbitals are divided into three categories based upon their energetics. The σ orbitals, corresponding to σ bonds, are the lowest energy occupied orbitals, with π orbitals lying at slightly higher energy levels and non-bonding orbitals with unshared pairs lying higher still. The unnoccupied π* and σ* orbitals represent the excited state.[71,72] These orbitals and their possible transitions are shown in Figure 5.

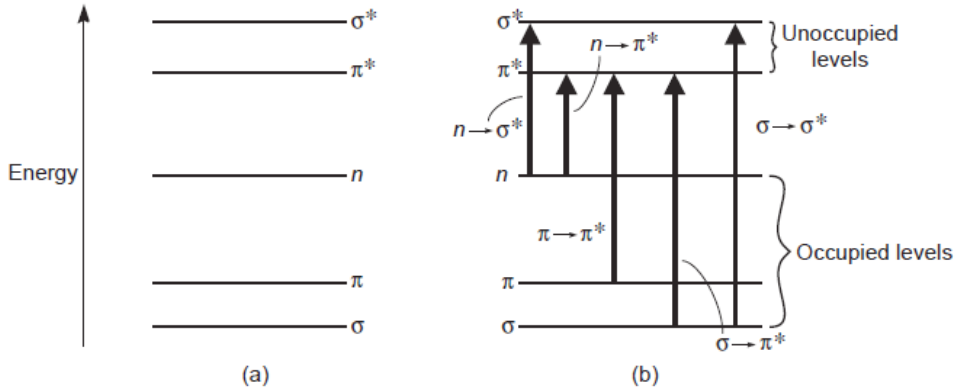

Figure 5. (a)Electronic energy levels and (b)transitions between states. [71]

For small molecules without unsaturation, transitions between energy levels generally require higher energy UV radiation. For systems with conjugated unsaturation, a bathochromic shift (red shift) is observed with increasing conjugation, as the increasing π conjugation allows for more possible π --> π* transitions with progressively smaller band gaps to occur. This effect is of great importance to the conjugated polymers in this study, as increased conjugation and the resulting bathochromic shift allows for viable use of these materials in harvesting longer λ light with lower energy. The optical band gap (E_{opt}) is calculated from the onset of the longest wavelength of the exciton absorption band (λ_{onset}), shown in Equation 2.[73] For polymers with extended π conjugation, the bathochromic shift can result absorption cutoffs and charge transfer peaks into the infrared region of the spectrum, necessitating characterization by FT-IR spectroscopy, which operates on many of the same principles as UV-Vis spectrophotometry.

$$E_{opt} = 1242/\lambda_{onset}$$

Equation 2. Calculation of optical band gap from onset wavelength.[73]

2.2.2 Cyclic Voltammetry

Cyclic voltammetry one of the most useful experiments that can be used to determine the electronic band gap of a organic material.[74] In these experiments, a triagnular voltage waveform is applied to a sample in solution and the current response is measured vs a reference electrode, generally saturated calomel or $Ag^{+}/AgCl$ in saturated KCl. The voltage waveform creates a linear potential sweep back and forth between two extremes known as switching potentials. The initial scan in CV can either be towards more negative potentials (forward scan) or towards more positive potentials (reverse scan) and may start at either extreme or a point in the middle.[75] The oxidation and reduction potentials extracted from cyclic voltammetry reveal the energy levels of the HOMO and LUMO, respectively. The HOMO represents how much energy is required to extract an electron from a molecule, while the LUMO represents how much energy is needed to inject an electron into the molecule. [76] After collecting the CV data for a sample, ferrocene is added to the test cell as a referencing standard in order to account for drift in the reference electrode. Once all collected data is standardized to the known redox potential of ferrocene vs the reference electrode being used, the estimated energy levels of the HOMO and LUMO are given by Equation 3. [77] The electonic band gap is the the difference between thee two values.

$$E(HOMO) = -e(E_{ox}^{onset} + 4.4)$$

$$E(LUMO) = -e(E_{red}^{onset} + 4.4)$$

Equation 3: Equations for calculation of the HOMO/LUMO energy levels.[77]

Chapter III. Experimental Methods

3.1 Synthetic Procedures

3.1.1 Synthesis of Donor

Linear (initially R = *n*-$C_{12}H_{25}$) solubilizing groups were chosen to minimize steric and electronic contributions and to promote sufficient solubility of the polymer products.[30] The coupling of dodecylzinc bromide with 3,5-dibromoaniline was performed via the use of a sterically bulky Pd–PEPPSI–IPent precatalyst as previously reported to form compound **D1**.[78]* This strategy should also provide access to a wide variety of functionalized derivatives for subsequent examination, as well as the benzylidene analogues. The reaction of 2,6-dibromo-4*H*-cyclopenta[2,1-*b*:3,4-*b*′]dithiophen-4-one with **D1** proceeded using $TiCl_4$ and triethylamine (NEt_3) in dichloromethane, producing the desired aryl imine-functionalized CPDT building block (**D2**). This compound was subsequently reacted with 3.5 equiv. of hexamethylditin $(SnMe_3)_2$ using $Pd(PPh_3)_4$ (10 mol%) in toluene at 80 °C to produce the corresponding stannane ($\boldsymbol{\pi_D}$).

3.1.2 Synthesis of Acceptor

The synthesis of the primary target of this research, the selenium derivatized acceptor and corresponding copolymer, is shown in Scheme 1. All synthetic procedures were done according to reported literature procedures of the sulfur analogue, with modifications where necessary. The sulfur analogue was first synthesized, reduced to a diamine, and selenated to form the benzoselenadiazole derivatives.

* Donor structures omitted for intellectual property purposes.

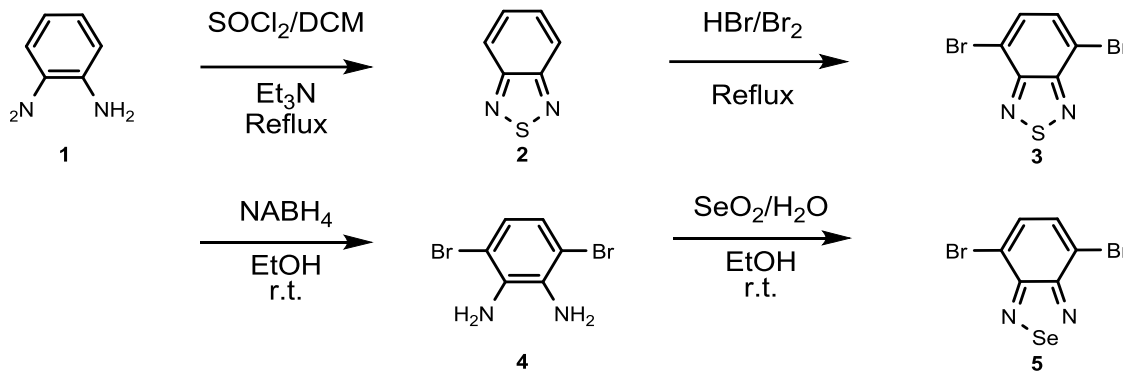

Scheme 1: Synthesis of acceptors

O-phenylenediamine (**1**) (5 g, 46.3 mmol) was dissolved in dichloromethane (80 mL) and triethylamine (21 mL, 150 mmol) in a round bottom flask and cooled to 0 ^{o}C using an ice bath. To this solution, thionyl chloride (8 mL, 110 mol) was added via a syringe and headed to reflux for 4hrs with stirring to give 2,1,3-benzothiadiazole (**2**) in >90% yield. Water was then added to quench excess thionyl chloride. The product formed an oil at the bottom of the reaction vessel. This oil was then removed with a separation funnel and residual solvent removed via rotary evaporation. Product **2** crystalized out upon cooling after rotary evaporation and was pure by TLC and ^{1}H NMR. **2** (5 g, 36.7 mmol) was then dissolved in HBr (75 mL, 1.38 mol) in a round bottom flask followed by dropwise addition of a Br_2 (17.7 g, 111 mmol) in HBr (16 mL, 294 mmol) at room temperature via an addition funnel while stirring. The mixture was then heated to 120^{o}C for 6 hours with stirring to yield 4,7-dibromo-2,1,3-benzothiadiazole (**3**) in >80% yield. The reaction mixture was quenched by pouring into ice water then collecting the precipitate via vacuum filtration. The filtrate was washed with 500mL of DI H_2O and dried overnight with vacuum. The crude 4,7-dibromo-2,1,3-benzoselenadiazole was then purified via filtration

through a plug of silica gel in a fritted filter funnel in a 1:1 mixture of dichloromethane and hexanes. **3** (8 g, 27.2 mmol) was added to EtOH (125 mL) in a round bottom flask at 0°C with stirring to form a slurry. Sodium borohydride (5 g, 132 mmol) was added to this slurry and the mixture was allowed to stir at room temperature for 6 hours to yield 3,6-dibromobenzene-1,2-diamine (**4**) in >80% yield. 20 mL DI H_2O was added to the reaction mixture to quench any residual sodium borohydride. The mixture was then filtered under reduced pressure to remove the insoluble precipitates. The remaining solution was then extracted three times with diethyl ether and dried via rotary evaporation. The diamine was purified via flash chromatography and solvent was removed via rotary evaporation. **4** (5 g, 18.8 mmol) was then dissolved in EtOH (100 mL) with stirring. Selenium dioxide (2.5 g, 1.2 equiv) was dissolved in DI H_2O (10 mL) and added dropwise to the solution of **4**. 4,7-dibromo-2,1,3-benzoselenadiazole (**5**) precipitate formed immediately. This precipitate was then collected via vacuum filtration and dried under vacuum and was pure by TLC in 1:1 DCM:hexanes and by ^{1}H NMR.

3.1.3 Polymerization

The synthetic approach for polymerization is shown in Scheme 2. Copolymerization of $\boldsymbol{\pi_D}$ with **3** (**P1**) and **5** (**P2**) were carried out via microwave heating using $Pd(PPh_3)_4$ (3–4 mol%) as the catalyst in xylenes[1,79,80] using a CME Discover-12 Hybrid microwave reactor with autosampler. This synthesis is shown in Scheme 2[1]

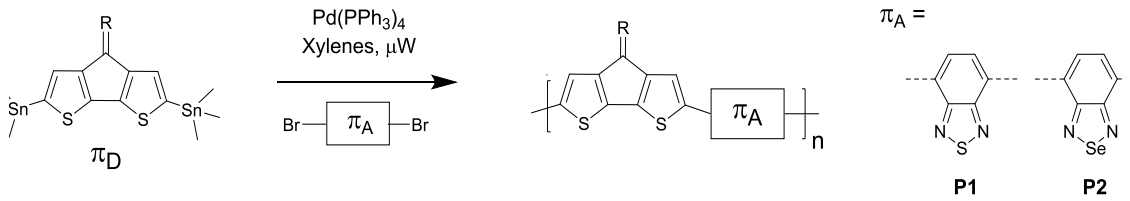

Scheme 2. Microwave mediated copolymerization reaction of donor with acceptors

3.2 Characterization

A Varian Mercury 300 MHz NMR spectrometer operating at a frequency of 300.13 MHz with VNMR 6.1C software was used to collect ^{1}H and ^{13}C NMR spectroscopies and assess the structures of the building blocks and polymeric materials. Absorption data in the infrared region of the spectrum was obtained using a Digilab Merlin FT-IR spectrophotometer. FT-IR studies were conducted by drop casting the polymer samples onto optical grade NaCl plates (25 mm x 4 mm) and scanning under a continuously purged nitrogen atmosphere at a resolution of 2 cm^{-1}. Film and solution UV-Vis absorption studies were conducted using an Agilent Technologies Cary 5000 UV-Vis-NIR spectrophotometer. The films were prepared by drop casting sample onto quartz slides. Solution samples were prepared through serial dilution of the polymer sample in chloroform until raw peak absorbance in a quartz cuvette was around 1 absorbance unit. Optical absorption data was then smoothed in OriginPro and normalized in Excel. Electrochemical measurements to assess the position of the frontier orbital energies were carried out through cyclic voltammetry (CV) using a Novocontrol Alpha Analyzer and Novocontrol POT/GAL 15 V/10 A potentiostat.

3.2.1 Establishing Operating Protocols for Cyclic Voltammetry

Prior to analyzing the polymers synthesized, it was necessary to establish the initial operating protocols for cyclic voltammetry experiments with the Novocontrol broadband dielectric spectrometry instruments. Initial experiments were carried out with donor-acceptor copolymers remaining from previous Azoulay Research Group studies. After several trials, it was found that 1 Dram borosilicate glass pressure relief reaction vials with supplied by Chemglass Life Sciences made the best electrochemical test cells due to their size and the ease of positioning electrodes through puncturing the pressure relief septa. Working and counter electrodes were made from 5 cm segments of platinum wire. To prevent damage to the soft platinum wire from contact with the alligator clips used to connect the cell, short copper leads were soldered to the platinum electrodes.

In order to ensure that both platinum electrodes are clean and ready for use, they are cleaned with acetone, polished with a dispersion of 25 μm diamond particles applied to a paper towel, washed with DI H_2O, dipped in dilute HCl for 10-15 seconds to remove trace oxidation, washed again with DI H_2O, then rinsed with acetone and dried under nitrogen immediately prior to use. Initial protocols were established using an Ag^+/AgCl reference electrode with a 3M NaCl filling solution and a porous glass frit. After several experiments, it was found that an Ag^+/AgCl reference electrode with a saturated KCl filling solution and a ceramic frit proved to give more consistent shifts in relation to the ferrocene standard.

Sample preparation proved difficult with some samples due to low solubility in $CHCl_3$. After several experiments, it was established that dissolving 5-10mg of polymer in minimal $CHCl_3$ in a 1 Dram vial with stirring and heating at 50 ^oC typically yielded the

best solutions for coating the electrodes. To qualitatively determine the appropriate solution concentrations, a small amount of solution was drawn up in a Pasteur pipette and examined. If a sample was transparent near the tip of the pipette, it was not concentrated enough to drop coat the electrode and excess solvent was evaporated with nitrogen flow. Once appropriate solution concentrations were achieved, the working electrode was pushed through the septa of the test cell cap. The cap was then removed so that the portion of the electrode beneath the septa could be coated. The solution used to coat the sample was left stirring at 50 ^{o}C on a hot plate to ensure proper concentration was maintained. The heated solution was drawn up into a Pasteur pipette and slowly dripped down the length of the wire (over the sample vial to recollect sample) until a homogenous film of the sample had been formed. Once the film on the working electrode was dried, the septa and cap were immediately placed on a 1 Dram vial from the drying oven and immediately pumped into the glove box to limit interactions with air and moisture.

Following the coating procedure, a 0.1 M solution of tetrabutylammonium hexafluorophospate in acetonitrile* (38.7 mg $TBAPF_6$ per mL ACN) was prepared in the glove box to act as the electrolyte in the test cell. For the 1 Dram test cell, 2.5 mL of the electrolyte solution was added. The test cell was removed from the glove box and immediately taken to sparge with argon to remove any residual oxygen from the test cell. While sparging, the working and reference electrodes were both inserted into the test cell and left to sparge for 5 minutes. The exit needle was removed just before the argon needle

* Initial experiments did not show appreciable differences in spectrums obtained from electrochemical grade acetonitrile when compared to spectrums from dry LC-MS grade acetonitrile. LC-MS was thus used for all diagnostic experiments.

was removed to maintain positive pressure and prevent the introduction of oxygen into the system.

Once sparged, the test cell was taken to the broadband dielectric spectrometer and connected to the potentiostat. The CV experiment was then configured in Novocontrol WinChem. After numerous experiments to optimize settings, it was established the best settings for the instrument setup were as follows:

- RE Setup: 3-Wire, 4.8 V range
- WE-Terminal: 1μA range, automatic range increase mode
- CE-Terminal: Potentiostat, current limit 1 A, voltage limit 4 V, connect from VCE

The best voltage waveform for polymer samples scans from 0 V to +1.5 V, down to -1.5 V, then back to 0 V over the course of 300 seconds for a scan rate of 20 mV/s with as many repetitions as necessary. This scan rate can be varied depending on the sample being run. The sample time was set to 100 ms to prevent the data files from becoming too large to process.

Following collection of all scans of the sample, a volume of ferrocene[*] in ACN was injected to the cell to reference the sample to a known redox potential and the scans were run again. The data was then saved as an ASCII file and worked up in Microsoft Excel and OriginLab OriginPro. After numerous initial experiments, it was discovered that all values collected by the instrument were reversed, therefore they must be multiplied by -1 in Excel to reverse the signs. Due to this reversal, the initial 0 V to +1.5 V scan is actually a forward scan from 0 V to -1.5 V. For the majority of CV experiments done, the third scan is the one of the most concern, so this scan is extracted in Excel and then normalized

[*] Qualitative, enough ferrocene was injected to add a slight yellow tint to the solution.

to the third scans of other samples in OriginPro. Following normalization, the onsets of the HOMO and LUMO are determined from the plots and the band gap energy levels are calculated as described in Equation 3.

3.2.2 Establishing Operating Protocols for FT-IR Spectroscopy

In order to characterize the absorption profiles of polymer samples in the infrared region of the electromagnetic spectrum, it was necessary to setup the Digilab Scimitar FT-IR instrument and establish operating procedures for it. Since the instrument was received without a sample holder, modifications were made to allow it to accept the solid sample holders from the Agilent Cary UV-Vis spectrophotometer. Once samples were able to be properly positioned, initial collection revealed that the ambient atmosphere in the building fluctuated too much for a stable background between samples. To remedy this, a nitrogen purge was setup to maintain a constant atmosphere inside the sample chamber. In order to ensure a stable atmosphere inside the instrument, it was established that the sample chamber should be purged for at least 5 minutes between being opened to insert a sample and beginning any type of data collection.

Initial experiments relied on drop-cast films from dilute polymer solutions in chloroform. Much like concentrations from CV, the concentrations of solutions for drop casting can be qualitative and varies between samples, with more soluble samples requiring lower concentrations to form uniform films. It was established that appropriate concentration of solution for a good drop-cast film could be determined by adding solvent to the solution until the polymer solution could be drawn into a Pasteur pipette and was still slightly transparent at the widest part. Once the solution was at the appropriate

concentration, 250 μL was drawn up in a micropipetter and applied to the surface of a clean salt plate until the entire surface was covered in solution. Often dragging the pipette tip across larger drops helped to aid in wetting the entire plate surface. For the most uniform films, solvent was allowed to dry slowly. The best established procedure for this is to coat the salt plates in a glove box and then allow the solvent to evaporate while purging the box with nitrogen. Allowing the solvent to evaporate too quickly (such as under direct nitrogen flow) left voids and fissures in the film, making it inadequate for FT-IR spectroscopy. Films formed from a properly diluted solution were completely transparent.

Data collection was done in Digilab Merlin 3.2 software. After a 5-10 minute purge with nitrogen, a background was collected at a resolution of 2 cm^{-1}. Following background collection, the sample was placed in the sample holder and the chamber was allowed to purge for another 5 minutes and then scanned 128 times at a resolution of 2 cm^{-1}. FT-IR data was then smoothed using boxcar averaging in the Merlin software, then exported as ASCII to be normalized in OriginPro and plotted in Excel.

3.2.3 Establishing Operating Protocols for UV-Vis

Following installation and instrument setup by Agilent technicians, the Cary 5000 UV-Vis-NIR spectrophotometer was ready for data collection. Though the instrument has the capabilities to run both a blank and a sample at once and then subtract the blank from the sample, this method causes problems when using unpaired cuvettes and unpaired quartz plates, as artifacts and noise from the blank can be incorrectly introduced into the sample spectrum. To remedy this, the instrument was blanked using a sample in only the front beam, then the samples were collected using only the front beam. For the most accurate

baseline measurements, the sample cuvette or slide was cleaned and then run alone to collect an accurate baseline to be subtracted from the sample spectrum. Films for UV-Vis can be drop cast in the same way as films for FT-IR, though spin coating gives much better results. The films for this study were drop cast onto quartz and annealed in the drying oven for 10 minutes at 120 ^{o}C. The solutions were made in chloroform and serially diluted until a peak absorbance of 0.5 to 1 AU was reached prior to normalizing.

After the data is collected, it was smoothed using boxcar averaging in the Cary software and then exported as ASCII to be worked up in Excel. Though the workup can be done in OriginPro, the default normalization can be lead to errors that are not introduced through manual normalization in Excel. Once the data was opened in excel, the baselines were subtracted and all spectra were normalized to a maximum within the desired range. This maximum was found using the maximum function in excel, with x-value restrictions set to limit the maximum only to the peak being analyzed.

Chapter IV. Results

The synthesized 4,7-dibromo-2,1,3-benzothiadiazole monomer was synthesized and purified to form off-white crystals. ^{1}H NMR (300 MHz, $CDCl_3$, 298 K) δ 7.76 (s, 2H, Ar-H) ^{13}C NMR (75 MHz, $CDCl_3$, 298 K) δ 153.1, 132.3, 113.9. The 4,7-dibromo-2,1,3-benzoselenadiazole monomer was purified to form a bright yellow powder, less soluble in most organics than the thiadizaole. ^{1}H NMR (300 MHz, $CDCl_3$, 298 K) δ 7.64 (s, 2H, Ar-H). ^{13}C NMR (75 MHz, $CDCl_3$, 298 K) δ 157.2, 132.1, 116.5. Once polymerized, **P1** (BT) formed a blue polymer while **P2** (BSe) formed a green polymer, consistent with the theoretical bathochromic shift associated with the heavier chalcogen. This is confirmed by UV-Vis spectrometry.

The UV-Vis absorption spectra of **P1** and **P2** are compared in Figure 6. These spectra illustrate broad absorption profiles with maxima (λ_{max}) in solution (25 ^{o}C in $CHCl_3$) occurring between 770 and 900 nm, red shifted from the maximum solar photon flux at ~700 nm.

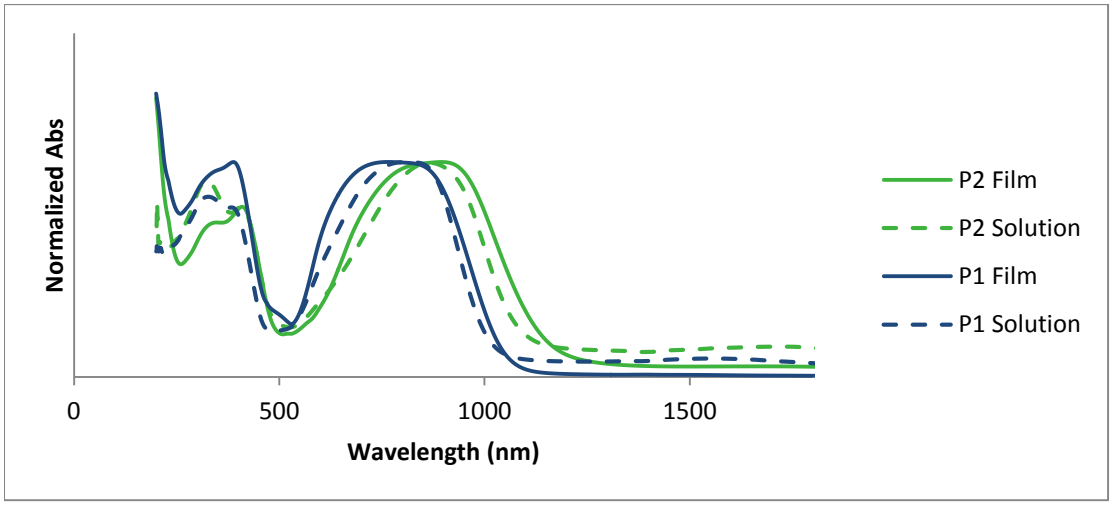

Figure 6. Normalized UV-Vis absorption spectra of **P1** and **P2** as film (solid) and in $CHCl_3$ solution (dashed).

The bathochromic shift in **P2** vs **P1** is indicative of a narrowing of the optical band gap due to the heavy atom effects of replacing the sulfur in **P1** with selenium in the case of **P2**. Excluding the Urbach tails, the peak onset of the **P1** film annealed at 120 ^{o}C for 10 minutes is ~1050 nm while **P1** in solution demonstrated an onset of ~1000 nm. Though bathochromically shifted, **P2** continued this trend with annealed film onset at ~1140 with the solution spectrum blue-shifted at ~1080 nm, about the same separation as observed in **P1**. The band gaps as calculated by equation 2 are shown in Table 1. Since the absorption profiles **P1** and **P2** did not extend into mid or far infrared, FT-IR spectra were not collected for these samples.

The absorption data plotted in eV (Figure 7) gives a visual representation of the optical band gaps of **P1** and **P2**. The optical band gaps of the material from the plot agree with the calculations done in Table 1.

Sample	λ_{onset} (nm)	E_{opt} (eV)
P1 Film	1050	1.18
P1 Solution	1000	1.24
P2 Film	1140	1.09
P2 Solution	1080	1.15

Table 1. Absorption onsets of **P1** and **P2** and the corresponding optical band gap calculations

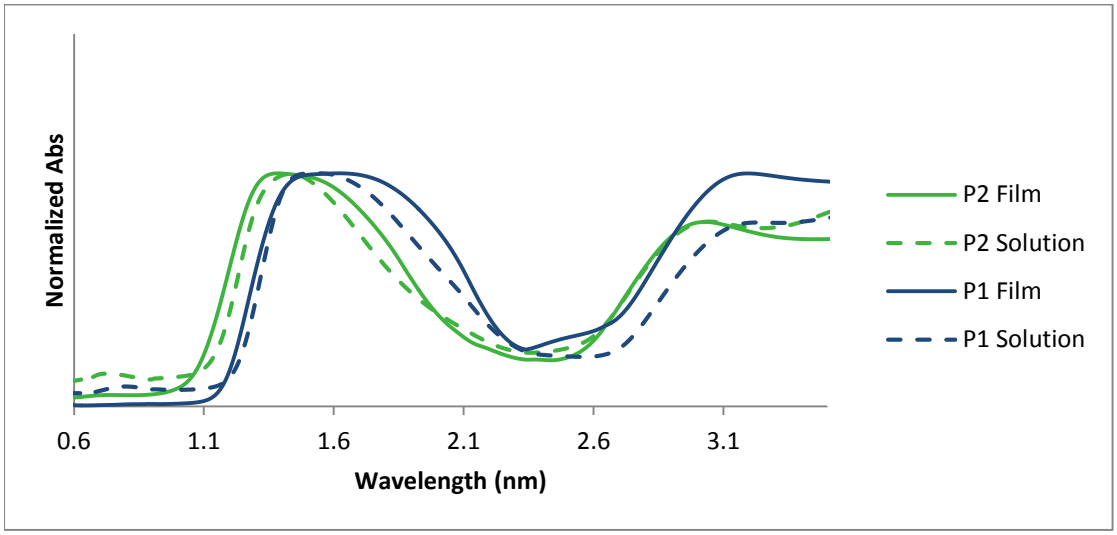

Figure 7. Normalized UV-Vis absorption spectra of **P1** (BT) and **P2** (BSe) plotted in eV.

The cyclic voltammetry experiments proceeded without issue and yielded measurements that line up well with the optical band gaps given from the spectrophotometry data. Both samples were quite stable under the experimental redox conditions, as indicated by the lack of amplitude degradation between scans 2-5 after the sample reached an equilibrium state after the first scan (Figure 8). The same scan with less stable materials typically results in amplitude degradation in successive scans as well as observable macroscopic physical degradation of the polymer film on the working electrode. Neither **P1** nor **P2** exhibited such degradation. The LUMO is significantly smaller in amplitude than the HOMO, indicating that these materials are both strongly p-type. This means that the donor-acceptor polymers have a greater electron hole concentration in the valence band than electron concentration in the conduction band.

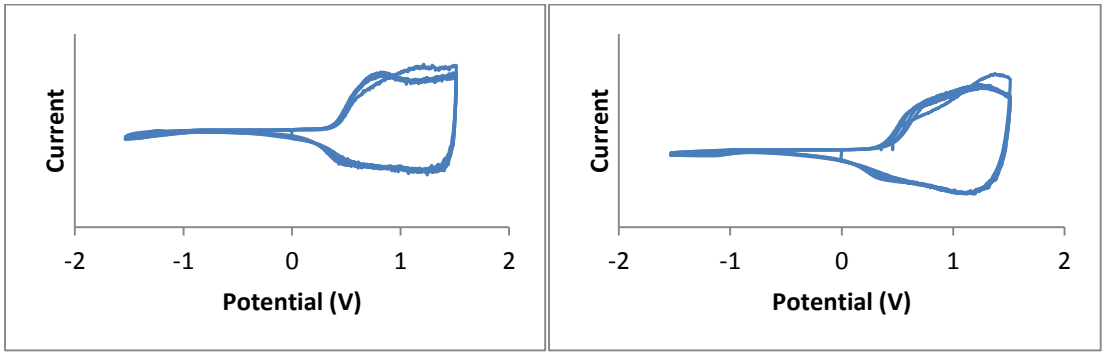

Figure 8: Raw 5 scan cyclic voltammograms of **P1** (left) and **P2** (Right)

Following the 5 scan cycle for each sample, ferrocene was added and referenced to a known value of 0.45 V vs Ag^{+}/AgCl in saturated KCl solution. For this reference process, the distance of the center of the ferrocene band gap (average of both peak maxima) to the known reference value was applied to all scans in order account for instrumental and reference electrode drift (demonstrated in Figure 9).

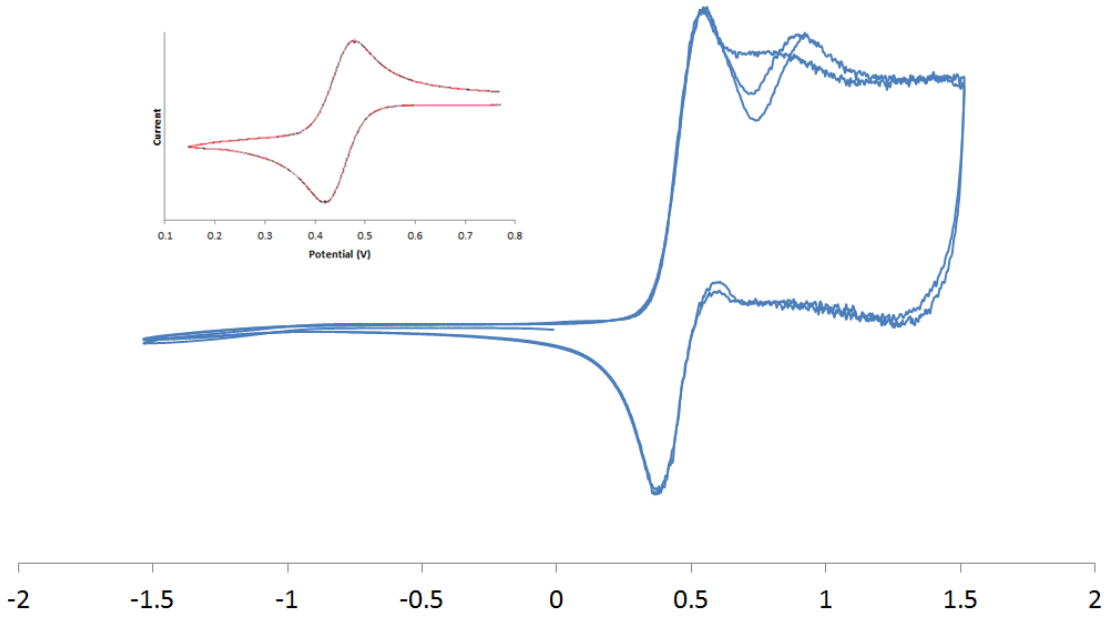

Figure 9: Top left: Sample CV of ferrocene. Center: Referencing of **P1** with ferrocene. The band gap of ferrocene for this set of scans is centered at 0.464V, requiring an adjustment of -0.014V to all scans of this sample.

The smoothed, normalized, and standardized third scan of each material was used for all band gap calculations (Figure 10). Based on these scans, prior to adjustment per Equation 3, **P1** had a HOMO onset of 0.305 V and a LUMO onset of -1.08 V while **P2** had a HOMO onset of 0.328 V and a LUMO onset of -0.969 V. Despite being narrower, the **P2** band gap sits at a slightly higher energy level than that of **P1**. The calculated band gap data from Equations 1-3 is found in Table 2. The values in Equation 4 accounted for ferrocene. Since this has been done separately, a value of 4.75 will be used in place of 4.4.

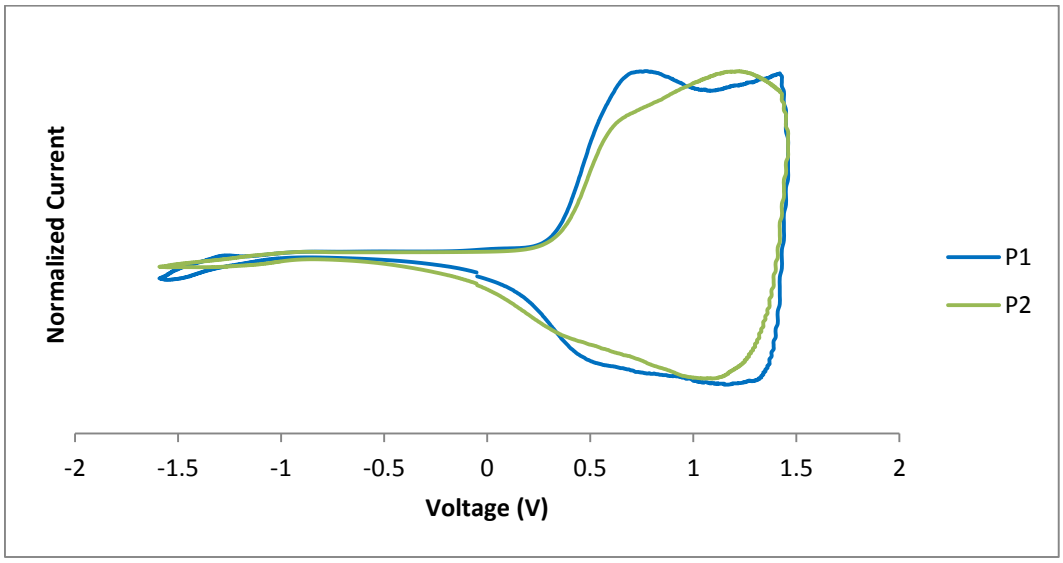

Figure 10: Standardized and normalized third scans of **P1** (BT) and **P2** (BSe).

Sample	HOMO (eV)	LUMO (eV)	λ_{onset} (nm)	E_{gap} (eV)	E_{opt} (eV)	E_B (eV)
P1 Film	5.05	3.67	1050	1.39	1.18	0.20
P2 Film	5.08	3.78	1140	1.30	1.09	0.21

Table 2: Calculation results for optical and electronic band gaps and exciton binding energies.

The data in Table 2 clearly indicates that the band gap of **P2** is lower than that of **P1** by nearly 0.1 eV. Based on Equation 1, the exciton binding energies in the film state

were nearly identical for both **P1** and **P2**. These calculations were only done in the film state since solution state cyclic voltammetry was not performed for these samples.

Chapter V. Conclusions

While the initially targeted selenium derivatized quinoxaline acceptor synthesis was not completed in the scope of this research, the polymers synthesized from 4,7-dibromo-2,1,3-benzothiadiazole and the corresponding derivatives indicate that future studies into the quinoxaline derivatives would be a worthwhile endeavor. The heavy atom effects of the selenium acceptor in conjunction with the proprietary CPDT donor yielded a copolymer with a narrower band gap than the previously established sulfur analogue. This polymer could have applications in light harvesting or detection in the edge of the near infrared region of the spectrum. Throughout the course of this research, standard operating protocols for FT-IR, UV-Vis, and CV characterization techniques, as well as the data workup process, were established to allow for proper characterization, analysis, and presentation of data collected from donor-acceptor copolymers in future studies.

References

1. Arias, A. C.; MacKenzie, J. D.; McCulloch, I.; Rivnay, J.; Salleo, A., Materials and Applications for Large Area Electronics: Solution-Based Approaches. *Chem. Rev.* **2010,** *110*, 3-24.
2. Chen, S.; Deng, L.; Xie, J.; Peng, L.; Xie, L.; Fan, Q.; Huang, W., Recent Developments in Top- Emitting Organic Light-Emitting Diodes. *Adv. Mater.* **2010,** *22*, 5227-5239.
3. Gelinck, G.; Heremans, P.; Nomoto, K.; Anthopoulos, T. D., Organic Transistors in Optical Displays and Microelectronic Applications. *Adv. Mater.* **2010,** *22*, 3778-3798.
4. Krebs, F. C., Fabrication and Processing of Polymer Solar Cells: A Review of Printing and Coating Techniques. *Sol. Energy Mater. Sol. Cells* **2009,** *93*, 394-412.
5. Geffroy, B.; le Roy, P.; Prat, C., Organic Light-Emitting Diode (OLED) Technology: Materials, Devices and Display Technologies. *Polym. Int.* **2006,** *55*, 572-582.
6. Guo, Y.; Yu, G.; Liu, Y., Functional Organic Field-Effect Transistors. *Adv. Mater.* **2010, 22**, 4427-4447.
7. Usta, H.; Facchetti, A.; Marks, T. J., N-Channel Semiconductor Materials Design for Organic Complementary Circuits. *Acc. Chem. Res.* **2011,** *44*, 501-510.
8. Dong, H.; Zhu, H.; Meng, Q.; Gong, X.; Hu, W., Organic Photoresponse Materials and Devices.*Chem. Soc. Rev.* **2012,** *41*, 1754-1808.
9. Li, G.; Zhu, R.; Yang, Y., Polymer Solar Cells. *Nat. Photon.* **2012,** *6*, 153-161.
10. Nelson, J., Polymer:Fullerene Bulk Heterojunction Solar Cells. *Mater. Today* **2011,** *14*, 462-470.
11. He, F.; Yu, L., How Far Can Polymer Solar Cells Go? In Need of a Synergistic Approach. *J. Phys. Chem. Lett.* **2011,** *2*, 3102-3113.

12. Azzellino, G.; Grimoldi, A.; Binda, M.; Caironi, M.; Natali, D.; Sampietro, M., Fully Inkjet- Printed Organic Photodetectors with High Quantum Yield. *Adv. Mater.* **2013,** *25*, 6829-6833.
13. Baeg, K. J.; Binda, M.; Natali, D.; Caironi, M.; Noh, Y. Y., Organic Light Detectors: Photodiodes and Phototransistors. *Adv. Mater.* **2013,** *25*, 4267-4295.
14. Wang, Z. Y., in *Near-Infrared Organic Materials and Emerging Applications*, CRC Press, Boca Raton **2013.**
15. Fabiano, S.; Musumeci, C.; Chen, Z.; Scandurra, A.; Wang, H.; Loo, Y. L.; Facchetti, A.; Pignataro, B., From Monolayer to Multilayer N-Channel Polymeric Field-Effect Transistors with Precise Conformational Order. *Adv. Mater.* **2012,** *24*, 951-956.
16. Rogalski, A., Infrared Detectors: An Overview. *Infrared Physics & Technology* **2002,** *43*, 187-210.
17. Fabian, J.; Nakazumi, H.; Matsuoka, M., Near-Infrared Absorbing Dyes. *Chem. Rev.* **1992,** *92*, 1197-1226.
18. Beverina, L.; Fu, J.; Leclercq, A.; Zojer, E.; Pacher, P.; Barlow, S.; Van Stryland, E. W.; Hagan, D. J.; Brédas, J.-L.; Marder, S. R., Two-Photon Absorption at Telecommunications Wavelengths in a Dipolar Chromophore with a Pyrrole Auxiliary Donor and Thiazole Auxiliary Acceptor. *J. Am. Chem. Soc.* **2005,** *127*, 7282-7283.
19. Qian, G.; Wang, Z. Y., Near-Infrared Organic Compounds and Emerging Applications. *Chem. Asian J.* **2010,** *5*, 1006-1029.
20. Kiyose, K.; Kojima, H.; Nagano, T.; Functional near-Infrared Fluorescent Probes. *Chem. Asian J.* **2008,** *3*, 506-515.
21. Holder, E.; Tessler, N.; Rogach, A. L., Hybrid Nanocomposite Materials with Organic and Inorganic Components for Opto-Electronic Devices. *J. Mater. Chem.* **2008,** *18*, 1064-1078.
22. Azoulay, J. D.; Koretz, Z. A.; Wong, B. M.; Bazan, G. C., Bridgehead Imine Substituted Cyclopentadithiophene Derivatives: An Effective Strategy for Band Gap Control in Donor– Acceptor Polymers. *Macromolecules* **2013,** *46*, 1337-1342.

23. Dang, M. T.; L. Hirsch; Wantz, G., P3HT: PCBM, Best Seller in Polymer Photovoltaic Research. *Adv. Mater.* **2011**, 23, 3597-3602.
24. Havinga, E. E.; ten Hoeve, W.; Wynberg, H., A New Class of Small Band Gap Organic Polymer Conductors. *Polym. Bull.* **1992,** *29*, 119-126.
25. Facchetti, A., π-Conjugated Polymers for Organic Electronics and Photovoltaic Cell Applications. *Chem. Mater.* **2011,** *23*, 733-758.
26. Zhou, H.; Yang, L.; You, W., Rational Design of High Performance Conjugated Polymers for Organic Solar Cells. *Macromolecules* **2012,** *45*, 607-632.
27. Gendron, D.; Leclerc, M., New Conjugated Polymers for Plastic Solar Cells. *Energy Environ. Sci.* **2011,** *4*, 1225-1237.
28. Tautz, R.; Da Como, E.; Limmer, T.; Feldmann, J.; Egelhaaf, H. J.; von Hauff, E.; Lemaur, V.; Beljonne, D.; Yilmaz, S.; Dumsch, I.; Allard, S.; Scherf, U., Structural Correlations in the Generation of Polaron Pairs in Low-Band gap Polymers for Photovoltaics. *Nat. Commun.* **2012,** *3*, 970.
29. Allard, S.; Forster, M.; Souharce, B.; Thiem, H.; Scherf, U., Organic Semiconductors for Solution-Processable Field-Effect Transistors (OFETs). *Angew. Chem. Int. Ed.* **2008,** *47*, 4070- 4098.
30. Wang, C.; Dong, H.; Hu, W.; Liu, Y.; Zhu, D., Semiconducting Pi-Conjugated Systems in Field- Effect Transistors: A Material Odyssey of Organic Electronics. *Chem. Rev.* **2012,** *112*, 2208- 2267.
31. Cheng, Y. J.; Yang, S. H.; Hsu, C. S., Synthesis of Conjugated Polymers for Organic Solar Cell Applications. *Chem. Rev.* **2009,** *109*, 5868-5923.
32. Gunes, S.; Neugebauer, H.; Sariciftci, N. S., Conjugated Polymer-Based Organic Solar Cells. *Chem. Rev*. **2007,** 107, 1324-1338
33. Brabec, C. J.; Sariciftci, N. S.; Hummelen, J. C., Plastic Solar Cells. *Adv. Funct Mater.* **2001,** 11, 15-26.
34. Clarke, T. M.; Durrant, J. R., Charge Photogeneration in Organic Solar Cells. *Chem. Rev.* **2010,** *110*, 6736-6767.
35. Wöhrle, D.; Meissner, D.; Organic Solar Cells. *Adv. Mater.* **1991**, 3, 129-138.

36. Tang, C. W.; Two-layer Organic Photovoltaic Pell. *Appl. Phys. Lett.* **1986,** 48, 183-5.
37. Halls, J. J. M.; Pichler, K.; Friend, R. H.; Moratti, S. C.; Holmes, A. B., Exciton Diffusion and Dissociation in a Poly(p-Phenylenevinylene)/C60 Heterojunction Photovoltaic Cell. *Appl. Phys. Lett.* **1996**, 68, 3120-3122.
38. Theander, M.; Yartsev, A.; Zigmantas, D.; Sundstrom, V.; Mammo, W.; Andersson, M. R.; Inganas, O., Photoluminescence Quenching at a Polythiophene/C60 Heterojunction. *Phys. Rev. B: Condens. Matter Mater. Phys.* **2000**, 61, 12957-12963.
39. Haugeneder, A.; Neges, M.; Kallinger, C.; Spirkl, W.; Lemmer, U.; Feldmann, J.; Scherf, U.; Harth, E.; Gugel, A.; Mullen, K., Exciton Diffusion and Dissociation in Conjugated Polymer/Fullerene Blends and Heterostructures. *Phys. Rev. B: Condens. Matter Mater. Phys.* **1999**, 59, 15346-15351.
40. Stubinger, T.; Brutting, W., Exciton Diffusion and Optical Interference in Organic Donor-Acceptor Photovoltaic Cells. *J. Appl. Phys.* **2001**, 90, 3632-3641.
41. Markov, D. E.; Amsterdam, E.; Blom, P. W. M.; Sieval, A. B.; Hummelen, J. C., Accurate Measurement of the Exciton Diffusion Length in a Conjugated Polymer Using a Heterostructure with a Side-Chain Cross-Linked Fullerene Layer. *J. Phys. Chem. A.* **2005**, 109, 5266-5274.
42. Zhang, Y.; Zhou, H.; Seifter, J.; Ying, L.; Mikhailovsky, A.; Heeger, A. J.; Bazan, G. C.; Nguyen, T. Q., Molecular Doping Enhances Photoconductivity in Polymer Bulk Heterojunction Solar Cells. *Adv. Mater.* **2013**, 25, 7038-7044.
43. Sariciftci, N. S.; Smilowitz, L.; Heeger, A. J.; Wudl, F., Photoinduced Electron Transfer from a Conducting Polymer to Buckminsterfullerene. *Science.* **1992**, 258, 1474-6.
44. Allemand, P. M.; Koch, A.; Wudl, F.; Rubin, Y.; Diederich, F.; Alvarez, M. M.; Anz, S. J.; Whetten, R. L., Two Different Fullerenes Have the Same Cyclic Voltammetry. *J. Am. Chem. Soc.* **1991**, 113, 1050-1051.
45. Brabec, C. J.; Zerza, G.; Cerullo, G.; De Silvestri, S.; Luzzati, S.; Hummelen, J. C.; Sariciftci, S., Tracing Photoinduced Electron Transfer Process in Conjugated

Polymer/Fullerene Bulk Heterojunctions in Real Time. *Chem. Phys. Lett.* **2001**, 340, 232-236.

46. Neugebauer, H.; Brabec, C. J.; Hummelen, J. C.; Janssen, R. A. J.; Sariciftci, N. S., Stability Studies and Degradation Analysis of Plastic Solar Cell Materials by Ftir Spectroscopy. *Synth. Met.* **1999**, 102, 1002-1003.
47. Neugebauer, H.; Brabec, C.; Hummelen, J. C.; Sariciftci, N. S., Stability and Photodegradation Mechanisms of Conjugated Polymer/Fullerene Plastic Solar Cells. *Sol. Energy Mater. Sol. Cells.* **2000**, 61, 35-42.
48. Singh, T. B.; Marjanovic, N.; Matt, G. J.; Guenes, S.; Sariciftci, N. S.; Montaigne Ramil, A.; Andreev, A.; Sitter, H.; Schwoediauer, R.; Bauer, S., High-Mobility N-Channel Organic Field-Effect Transistors Based on Epitaxially Grown C60 Films. *Org. Electron.* **2005**, 6, 105-110.
49. Backer, S. A.; Sivula, K.; Kavulak, D. F.; Fréchet, J. M. J., High Efficiency Organic Photovoltaics Incorporating a New Family of Soluble Fullerene Derivatives. *Chem. Mater.* **2007**, 19, 2927-2929.
50. Riedel, I.; von Hauff, E.; Parisi, J.; Martin, N.; Giacalone, F.Dyakonov, V., Diphenylmethanofullerenes: New and Efficient Acceptors in Bulk-Heterojunction Solar Cells. *Adv. Funct. Mater.* **2005**, 15, 1979-1987.
51. Popescu, L. M.; van't Hof, P.; Sieval, A. B.; Jonkman, H. T.; Hummelen, J. C., Thienyl Analogue of 1-(3-Methoxycarbonyl) Propyl-1-Phenyl-[6, 6]-Methanofullerene for Bulk Heterojunction Photovoltaic Devices in Combination with Polythiophenes. *Appl. Phys. Lett.* **2006**, 89, 213507.
52. Xu, Z.; Chen, L. M.; Yang, G.; Huang, C. H.; Hou, J.; Wu, Y.; Li, G.; Hsu, C. S.; Yang, Y., Vertical Phase Separation in Poly (3-Hexylthiophene): Fullerene Derivative Blends and Its Advantage for Inverted Structure Solar Cells. *Adv. Funct. Mater.* **2009**, 19, 1227-1234.
53. Hummelen, J. C.; Knight, B. W.; LePeq, F.; Wudl, F.; Yao, J.; Wilkins, C. L., Preparation and Characterization of Fulleroid and Methanofullerene Derivatives. *J. Org. Chem.* **1995**, 60, 532-538.

54. Wienk, M. M.; Kroon, J. M.; Verhees, W. J. H.; Knol, J.; Hummelen, J. C.; van Hal, P. A.; Janssen, R. A. J., Efficient Methano[70]Fullerene/Mdmo-Ppv Bulk Heterojunction Photovoltaic Cells. *Angew. Chem., Int. Ed.* **2003**, 42, 3371-3375.
55. Yao, Y.; Liang, Y.; Shrotriya, V.; Xiao, S.; Yu, L.Yang, Y., Plastic near-Infrared Photodetectors Utilizing Low Band Gap Polymer. *Adv. Mater.* **2007**, 19, 3979-3983.
56. Arbogast, J. W.; Foote, C. S., Photophysical Properties of C70. *J. Am. Chem. Soc.* **1991**, 113, 8886-8889.
57. Zhu, Z.; Waller, D.; Gaudiana, R.; Morana, M.; Mühlbacher, D.; Scharber, M.; Brabec, C., Panchromatic Conjugated Polymers Containing Alternating Donor/Acceptor Units for Photovoltaic Applications. *Macromolecules.* **2007**, 40, 1981-1986.
58. Gong, X.; Tong, M. H.; Park, S. H.; Liu, M.; Jen, A.; Heeger, A. J., Semiconducting Polymer Photodetectors with Electron and Hole Blocking Layers: High Detectivity in the near-Infrared. *Sensors (Basel).* **2010**, 10, 6488-6496.
59. Grancini, G.; Maiuri, M.; Fazzi, D.; Petrozza, A.; Egelhaaf, H.J.; Brida, D.; Cerullo, G.Lanzani, G., Hot Exciton Dissociation in Polymer Solar Cells. *Nat. Mater.* **2013**, 12, 29-33.
60. Gibson, G.L.Seferos, D.S., "Heavy-Atom" Donor–Acceptor Conjugated Polymers. *Macromolecular Chemistry and Physics.* **2014**, 215, 811-823.
61. Kronemeijer, A.J.; Gili, E.; Shahid, M.; Rivnay, J.; Salleo, A.; Heeney, M.Sirringhaus, H., A Selenophene-Based Low-Band gap Donor–Acceptor Polymer Leading to Fast Ambipolar Logic. *Adv Mater.* **2012**, 24, 1558-1565.
62. Patra, A.; Wijsboom, Y. H.; Leitus, G.; Bendikov, M. Tuning the Band Gap of Low-Band-Gap Polyselenophenes and Polythiophenes: The Effect of the Heteroatom. *Chem. Mater.* **2011**, 23, 896−906.
63. Smyth, C.; Lewis, G.; Grossman, A.; Jennings, F., III The Dipole Moments and Structures of Certain Compounds of Sulfur, Selenium and Phosphorus. *J. Am. Chem. Soc.* **1940**, 62, 1219−1223.

64. Kamada, K.; Ueda, M.; Nagao, H.; Tawa, K.; Sugino, T.; Shmizu, Y.; Ohta, K. Molecular Design for Organic Nonlinear Optics: Polarizability and Hyperpolarizabilities of Furan Homologues Investigated by Ab Initio Molecular Orbital Method. *J. Phys. Chem.* **2000**, 104, 4723−4734.
65. Zhuang, W.; Zhen, H.; Kroon, R.; Tang, Z.; Hellström, S.; Hou, L.; Wang, E.; Gedefaw, D.; Inganäs, O.; Zhang, F.; et al. Molecular Orbital Energy Level Modulation through Incorporation of Selenium and Fluorine into Conjugated Polymers for Organic Photovoltaic Cells. *J. Mater. Chem.* **2013**, 1, 13422−13425.
66. Jiang, J.-M.; Raghunath, P.; Lin, H.-K.; Lin, Y.-C.; Lin, M.; Wei, K.-H. Location and Number of Selenium Atoms in Two-Dimensional Conjugated Polymers Affect Their Band-Gap Energies and Photovoltaic Performance. *Macromolecules* **2014**, 47, 7070−7080.
67. Alghamdi, A. A.; Watters, D. C.; Yi, H.; Al-Faifi, S.; Almeataq, M. S.; Coles, D.; Kingsley, J.; Lidzey, D. G.; Iraqi, A. Selenophene vs. Thiophene in Benzothiadiazole-Based Low Energy Gap Donor−Acceptor Polymers for Photovoltaic Applications. *J. Mater. Chem.* **2013**, 1, 5165−5171.
68. Acharya, R.; Cekli, S.; Zeman, C.; Altamimi, R.; Schanze, K. Effect of Selenium Substitution on Intersystem Crossing in π-Conjugated Donor–Acceptor–Donor Chromophores: The LUMO Matters the Most. *J. Phys. Chem. Lett*., **2016**, 7 (4), 693–697
69. Sun, S. S.; Sariciftci, N. S.; *Organic Photovoltaics: Mechanisms, Materials, and Devices,* 5th ed.; CRC Press, **2005**; pp 202-220
70. Winder, C.; Sariciftci, N. S. Low Bandgap Polymers for Photon Harvesting in Bulk Heterojunction Solar Cells. *J. Mater. Chem.,* **2004**, 14, 1077-1086
71. Pavia, D,; Lampman, G.; Kriz, G.; Vyvyan, J. *Introduction to Spectroscopy,*4th ed. Brooks Cole, **2008**; pp 370-400.
72. Shehzad, S. Optical Spectroscopic and theoretical investigations of a series of fluoroquinolones. Roskilde University, Denmark. **2010.**
73. Djurovich, P. I.; Mayo, E. I.; Forrest, S. R.; Thompson, M. E. Measurement of the Lowest Unoccupied Molecular Orbital Energies of Molecular Organic Semiconductors. *Organic Electronics*. **2009.** pp 515–520

74. Branzoi, I. V.; Leonat, L.; Sbarcea, G. Cyclic Voltammetry for Energy Levels Estimation of Organic Materials. *Sci. Bull. B. Chem. Mater. Sci.* **2013**.
75. Skoog, D. A.; Holler, F. J.; Nieman, T. A.; *Principles of Instrumental Analysis,* 6th ed. Saunders College Pub, Philadelphia. **1998**.
76. Antohe, S. *Organic Materials and Electronic Devices*. University of Bucharest. **1996**.
77. Bredas, J. L.;Silbey, R.; Boudreux, D. S.; Chance, R. R. Chain-length dependence of electronic and electrochemical properties of conjugated systems: polyacetylene, polyphenylene, polythiophene, and polypyrrole, *J. Am. Chem. Soc.* **1983**, 105, 6555.
78. Calimsiz, S.; Organ, M. G., Negishi Cross-Coupling of Secondary Alkylzinc Halides with Aryl/Heteroaryl Halides Using Pd-Peppsi-Ipent. *Chem. Commun.* . **2011**, 47, 5181-5183.
79. Pilgram, K.; Zupan, M.; Skiles, R., Bromination of 2,1,3-benzothiadiazoles. *J. Heterocyclic Chem*. **1970,** 7, 629–633
80. Susumu, K.; Duncan, T.V.Therien, M. J., Potentiometric, Electronic Structural, and Ground- and Excited-State Optical Properties of Conjugated Bis[(Porphinato)Zinc(II)] Compounds Featuring Proquinoidal Spacer Units. *J. Am. Chem. Soc.* **2005**, 127, 5186-5195.